Chalmers Publication Library

Copyright Notice

(Article begins on next page)

Resistive Graphene FET Subharmonic Mixers: Noise and Linearity Assessment

Michael A. Andersson, *Student Member, IEEE,* Omid Habibpour, *Student Member, IEEE,*
Josip Vukusic, *Member, IEEE,* and Jan Stake, *Senior Member, IEEE*

Abstract—We report on the first complete RF characterization of graphene FET subharmonic resistive mixers in the frequency interval f_{RF} = 2-5 GHz. The analysis includes conversion loss, noise figure and intermodulation distortion. Due to an 8 nm thin Al_2O_3 gate dielectric the devices operate at only $\sim$0 dBm of local oscillator power, with an optimum measured conversion loss in the range 20-22 dB. The noise figure closely mimics the conversion loss, thus determining the noise to be essentially thermal in origin, which is promising for cryogenic applications. The highest input third order intercept point is measured to be 4.9 dBm at a local oscillator power of 2 dBm.

Index Terms—Graphene, FETs, subharmonic resistive mixers, noise measurements, intermodulation distortion.

I. INTRODUCTION

GRAPHENE has recently attracted great attention in the field of nanotechnology aimed at RF- and microwave electronics [1], [2]. This was made possible by the first isolation of graphene, a one-atom layer sheet of carbon atoms organized in a honeycomb lattice, together with the demonstration of the field-effect, in 2004 [3]. Since, the graphene synthesis methods have advanced, making it a promising candidate comparing to e.g. carbon nanotubes (CNTs). The potential for FETs, derived from graphenes high intrinsic carrier mobility for both electrons and holes, 100,000 cm^2/Vs, and the high carrier saturation velocities of $4-5\cdot 10^7\ cm/s$ has been thoroughly investigated, as recently reviewed in [4]. Ultimately, G-FETs with f_T and f_{max} in excess of 1 THz are projected, in the limit of channel length down-scaling and eliminating the currently deteriorating device parasitics [2]. Moreover, graphene has the unique property to switch between the n- and p-channel by electrical gating and distinctive properties useful in e.g. optoelectronics [5] and sensor applications [6].

Since the realization of the first top-gated graphene field effect transistor (G-FET) in 2007 [7] there have been considerable efforts to go to higher frequencies. The high-frequency capabilities demonstrated are far from the intrinsic potential, with published $f_{max} \leq 35$ GHz [8]. Suitability of G-FETs for microwave circuit applications has been investigated, resulting in high spectral purity frequency multipliers [9], fundamental

transconductance mixers [10], [11] with a best conversion loss (CL) of 27 dB at 4 GHz, a subharmonic resistive mixer with a CL of 24 dB [12] at 2 GHz and a 10-dB small-signal power amplifier operating at 1 GHz [13]. In addition, an RF rectifying detector, with a linear and high dynamic range response up to 50 GHz [14] has been presented. While GaAs FET active mixers can provide 6-10 dB conversion gain [15], resistive G-FET mixers are behind mature GaAs HEMT counterparts, where fundamental [16] and subharmonic [18] designs achieve CL of 5.3 dB and 6.5 dB, respectively. Further performance analysis beyond measuring the CL, in terms of noise and intermodulation performance is still sparse for G-FET mixers, with a single value for input third order intercept point (*IIP3*) of 13.8 dBm reported at 10 MHz for a fundamental transconductance mixer [10].

In this paper, we expand the characterization for the G-FET resistive subharmonic mixer of [19], which included CL and noise figure (NF). This represented the first study of noise at microwave frequencies for a G-FET, while previous studies considered only low frequency $1/f$ noise and phase noise [20]. The addition includes intermodulation distortion (IMD) of the mixer as examined via two-tone measurements to extract the *IIP3*, which besides the CL and NF represents the most important quantity to study for a microwave mixer, from a systems perspective. Finally, the large signal model of [21] is utilized to validate the IMD results.

II. MOTIVATION FOR RESISTIVE G-FET MIXERS

There are basically two operating principles for a FET mixer; either utilizing the change in transconductance, g_m, or channel conductance (resistance), G_{ds} (R_{ds}), with gate source voltage. In both approaches a local oscillator (LO) signal is applied to the gate to achieve a resulting time-varying, periodic quantity $g_m(t)$ or $G_{ds}(t)$. The former case is referred to as an active transconductance mixer, where the RF signal is applied to the gate, and the latter a resistive mixer, with the RF signal applied to the drain. The LO pumped time-varying quantity, either g_m or G_{ds}, may be expressed as a Fourier cosine series in terms of LO frequency harmonics $g(t)$ [22],

$$g(t) = g_0 + 2\sum_{n=1}^{\infty} g_n \cos n\omega_{LO}t, \qquad (1)$$

where the first order coefficient g_1 of $\cos \omega_{LO}t$ is responsible for the efficiency of fundamental mixing and second order coefficient g_2 for subharmonic mixing.

Best possible performance from a transconductance mixer is realized by maximizing the variation in g_m, which is accomplished by biasing the FET in current saturation [15]. Under these conditions the active FET mixer can provide a maximum conversion gain expressed with its small-signal circuit elements and the g_1 coefficient as [22],

$$G_c = \frac{g_1^2 R_{ds}}{4\omega_{RF}^2 C_{gs}^2 R_{in}}.$$ (2)

Contrary to active mixers, for a resistive mixer the drain is unbiased. It is limited to a conversion loss, which was analyzed in [16], with the aim of acquiring an intuitive expressions in terms of device parameters, for understanding of the mixer operation and preliminary design work. The analysis is done in terms of the reflection coefficient as seen from the drain port, $\Gamma(t) = (R_{ds}(t) - Z_0)/(R_{ds}(t) + Z_0)$. This assumes that all mixing terms are terminated in a matched load, the real system impedance, Z_0. The best performance assumes $\Gamma(t)$ to be a 0.5 duty-cycle square wave and yields,

$$CL_{square} = \frac{\pi^2}{(\Gamma_{max} - \Gamma_{min})^2}.$$ (3)

Further, the ideal case with $\Gamma_{max} = 1$ and $\Gamma_{min} = -1$, corresponding to resistance states $R_{max} = \infty$ and $R_{min} = 0$, results in a minimum CL of 3.9 dB. This is to be compared to a CL of 3 dB for an ideal double-sideband mixer with all terms except the image ideally terminated and a CL of 0 dB if also the image is reactively terminated [17]. Since the mixing is related to the g_1 coefficient of (1), in addition to the on-off ratio, the CL decreases with an alteration of the $R_{ds}(t)$ waveshape. Making the time varying shape triangular instead yields,

$$CL_{triangular} = \frac{\pi^2}{4}\frac{\pi^2}{(\Gamma_{max} - \Gamma_{min})^2},$$ (4)

which is consistent with the fact that $g_{1,square} > g_{1,triangular}$.

As a consequence of the currently low transconductance in G-FETs and the lack of clear current saturation, the so far reported G-FET transconductance mixers have shown poor performance, with a high CL. Instead, presently it is more promising to use the resistive mixing concept. Importantly, it currently also makes the best utilization of the unique transport properties of graphene for a novel concept, to do subharmonic mixing with a single FET. The extension to a subharmonic resistive design in conventional FETs is done e.g. by a parallel configuration where the LO is applied $180°$ out of phase to the gates of two devices [18]. Since this requires a balun, the G-FET subharmonic mixer allows a more compact circuit.

III. DEVICE DESIGN AND FABRICATION

The device design was focused on minimizing the mixer conversion loss. Since $CL \propto 1/(\Gamma_{max} - \Gamma_{min})^2$ [11] for resistive mixers, the above discussion translates this into a high on-off ratio, i.e. $R_{min} \ll Z_0$ and $R_{max} \gg Z_0$. This is true also for the timevarying waveshape resulting from symmetric transfer characteristics of a G-FET. In order to optimize the conditions for our G-FET resistive mixer, the
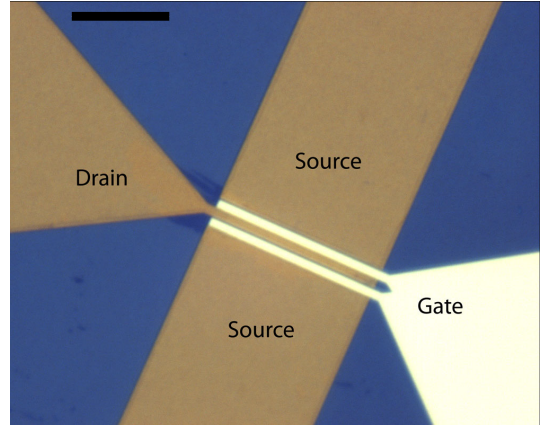

Fig. 1: Optical image of fabricated device with two gate fingers, yielding $W_g = 2 \times 15 \ \mu m$. Scale bar is $10 \ \mu m$.

device dimensions are chosen to be $L_g = 1 \ \mu m$ and $W_g = 30 \ \mu m$ based upon the reasoning in [12].

The actual devices were fabricated on graphene flakes produced by mechanical exfoliation on 300 nm silicon dioxide. The drain and source pads were formed via an electron beam lithography exposure and subsequent evaporation of 1 nm Ti, 15 nm Pd and 60 nm Au and lift-off. The thin layer of Ti is used for improved adhesion, while the Pd layer is known to simultaneously provide good contact resistivity and symmetric transfer characteristics. A stepwise natural oxidation, while heated on a hotplate, of electron beam evaporated Al was used to grow an 8 nm thick Al_2O_3 gate oxide. The aim was to reduce the LO power requirement compared to previous work, since the higher gate capacitance per area reduces the required gate swing voltage. A second electron beam lithography step was used to define a top-gate electrode, which uses a similar metalization stack with more Ti consisting of 4 nm Ti, 15 nm Pd and 60 nm Au.

The above described methods were used to fabricate three devices with slightly different performance, as will be subsequently indicated. Device #1 was used for original noise figure characterization first presented in [19] and device #2 was produced for the intermodulation analysis of this extended paper. Since device #2 had a too high leakage current, the gate voltage analysis was performed with device #3, with the main purpose of comparison to model simulations. A magnified optical photo of a two-finger G-FET device characterized in this paper is shown in Fig. 1.

IV. RF MEASUREMENT SETUPS

The mixer operation is based on a sinusoidal LO signal applied to the gate of the G-FET, biased at the point of minimum conductivity (Dirac voltage). Due to the electron-hole duality of the graphene channel conduction, the on and off states are swept twice in one LO cycle and the resistance variation as seen from the drain, $R_{ds}(t)$, has a fundamental frequency component at twice f_{LO}. Thus, the multiplication with f_{RF}, applied to the drain terminal, contains terms of the form $|f_{RF} \pm 2n \times f_{LO}|$, including the desired
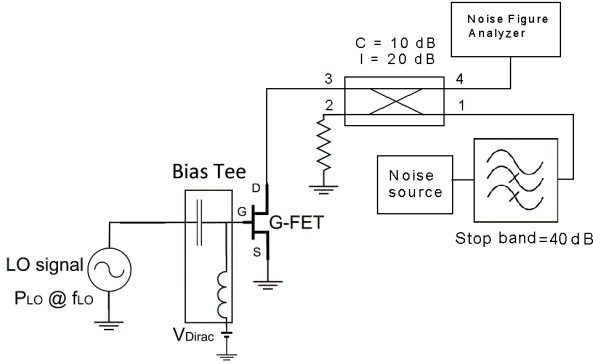
Fig. 2: Setup for measuring the G-FET subharmonic mixer noise figure in a 50 Ω system. Details are in Section IV-A.

Fig. 3: Two-tone measurement setup for examination of the G-FET subharmonic mixer intermodulation distortion ($IIP3$) in a 50 Ω system. The details are outlined in Section IV-B.

intermediate frequency component for subharmonic down-conversion $f_{IF} = |f_{RF} - 2f_{LO}|$ [12], with the frequency spacing utilized to separate the RF and IF signals at the drain. All RF measurements were performed on chip using a probe station.

A. Noise figure measurement setup

The complete measurement setup for the mixer noise is shown in Fig. 2, the core being the Agilent N8975A noise figure analyzer (NFA). It was used to determine both the conversion loss and noise figure versus frequency in the range $f_{RF} = $ 2-5 GHz, with the measurement frequency set to $f_{IF} = $ 100 MHz. The system was calibrated to account for the noise generated by the NFA itself and also the known losses in the setup on the signal path from the noise source to the NFA. A broadband noise source, with $ENR = 15$ dB $\pm$ 0.1 dB in the relevant frequency range, was utilized to increase the Y-factor, and thus the measurement accuracy. The signal separation at the drain terminal was performed with a directional coupler having 10 dB coupling in the frequency range 1-18 GHz. The RF noise signal is coupled to the drain of the G-FET and the reflected signal at $f_{IF} = 100$ MHz is transmitted directly to the NFA, since it is out of the coupler bandwidth. Similarly, noise in the measurement bandwidth originating from the matching termination connected at port 2 is not coupled to the NFA. An additional 40 dB isolation between port 1 and port 4 at the measurement frequency of 100 MHz is provided by an external SMA high-pass filter, to assure that the measured noise originates from the mixer and not the noise source. The filter characteristic is flat up to 5 GHz, which sets the upper limit on the measurement frequency.

B. IIP3 measurement setup

The well-established two-tone measurement principle [15] is used for the IMD measurement as presented in Fig. 3. The setup thus uses in total three signal generators. The two equal-power RF signals are chosen to be at closely spaced frequencies and separated by 20 MHz, e.g. $f_{RF,1} = 2.11$ GHz and $f_{RF,2} = 2.09$ GHz. With a standard power combiner at port 1 of the directional coupler the two RF signals are coupled to the drain of the G-FET, connected at port 3. The directional
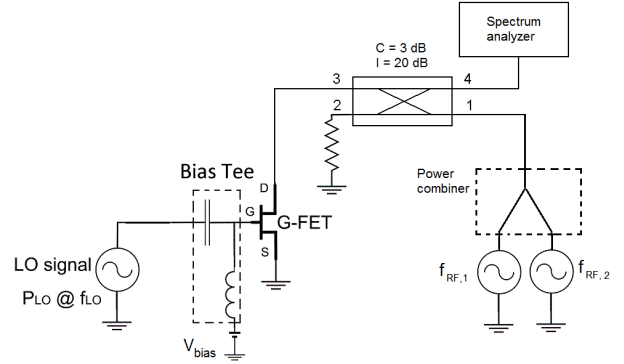
coupler has a 3 dB coupling factor to allow for high enough input powers to the mixer needed to detect the weak third order response. The resulting lower frequency signals are transmitted directly from port 3 to port 4 of the coupler and monitored with a spectrum analyzer. The expected down-converted linear responses while pumping with frequency $f_{LO} = 1$ GHz are at the frequencies $f_{IF,1} = 110$ MHz and $f_{IF,2} = 90$ MHz and the corresponding third order IMD responses are consequently at $2f_{IF,1} - f_{IF,2} = 130$ MHz and $2f_{IF,2} - f_{IF,1} = 70$ MHz. The same intermediate and third order intermodulation frequencies were used to measure in the interval $f_{RF} = $ 2-4 GHz. Port 2 of the directional coupler is again terminated in a matched load, $Z_0 = 50$ Ω. First, a verification of the integrity of the measurement setup was done, to ascertain that the signals at 130 MHz and 70 MHz originate from the device and not from mixing of the outputs between different harmonics of the signal generators. Connecting the spectrum analyzer directly to the output of the power combiner, only the two fundamental tones were observed for the relevant input signal levels.

V. MEASUREMENT RESULTS AND DISCUSSION

To evaluate the mixing capabilities of the fabricated devices a DC characterization is made. The main purpose is to find the drain to source resistance as presented in Fig. 4, for both devices together with the model fitted curves [21]. The devices exhibit different on-off ratios $R_{max}/R_{min} = 170/60 \approx 2.8$, $R_{max}/R_{min} = 130/35 \approx 3.7$ and $R_{max}/R_{min} = 150/60 = 2.5$, respectively, with the other parameters summarized in Table I. Mainly the contact resistances and mobilities differ, while device #2 exhibits a slightly larger asymmetry with $R_{ext} \approx 8$ Ω. A gate oxide capacitance of 0.5 $\mu F/cm^2$ is achieved for all devices. To reach $R_{min} = R_0$, a larger gate voltage swing is required, which increases the gate leakage and with possible risk of dielectric breakdown. The corresponding gate leakage for device #1, for which the NF measurement was performed, was $I_g \leq 20$ pA, which eliminates the shot noise and $1/f$ noise in FET resistive mixers [23]. The small shift of the Dirac voltage is beneficial for the mixer to operate at zero gate bias. Also, the asymmetry around V_{dirac} is small, which is important for the subharmonic mixing capability.

TABLE I: Summary of device parameters used for simulations

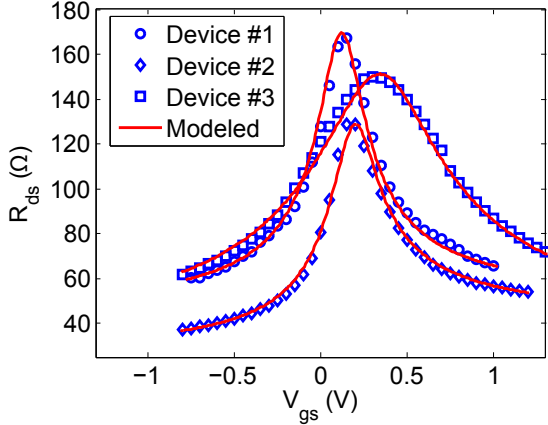|	R_c (Ω)	μ_e (cm^2/Vs)	μ_h (cm^2/Vs)	R_{ext} (Ω)
Device #1	21	1750	1750	3
Device #2	12	2550	2600	8
Device #3	14	800	900	1

Fig. 4: Corresponding resistance swept by the LO in mixer operation for the devices at $V_{ds} = 0.1$ V, together with the modeled resistance curves used in the simulations.

A. Mixer noise figure

The resulting conversion loss and noise figure for the mixer, given by device #1, in the frequency range $f_{RF} = 2$-5 GHz are shown in Fig. 5 as measured by the NFA. The conversion loss lies in the interval 20-22 dB (± 1 dB) and was verified at $f_{RF} = 2$ GHz using a spectrum analyzer. The high conversion loss is limited by the uneven distribution in time of R_{max} and R_{min} and the waveform shape. This requires a higher on-off ratio to reach the same performance as conventional fundamental resistive FET mixers [16]. Due to the thin gate dielectric, the required LO power was merely $P_{LO} = 0$ dBm, a significant improvement to $P_{LO} = 15$ dBm in [12]. The operating frequency interval corresponds to the best reported G-FET mixers, while conversion loss represents a state-of-the-art result [11], [12], [24].

The noise figure presented in Fig. 5 is single-sideband (SSB) after applying a 3 dB correction to the measured double-sideband (DSB) quantity, which is valid as outlined in the analysis of mixer noise figure below. The SSB noise figure is greater than the conversion loss by ≤ 1 dB, with an estimated measurement accuracy of ± 2 dB according to the investigation in [25]. At this high conversion loss, the accompanying noise figure must be high in order to be measured, but still the result is sensitive to imperfections in the setup. The error is mainly attributed to mismatch at the drain, which is approximately equal at f_{RF} and f_{IF} due to the low frequency. Harmonic balance simulations using the large signal model in [21] predicts the RF and IF impedances presented by the mixer to be 100 Ω, which yields $VSWR = 2$ with $Z_0 = 50$ Ω.

Despite the measurement uncertainty, there is clearly a close correlation between conversion loss and noise figure, $F_{mixer,SSB} \approx CL$. This relation between conversion loss and
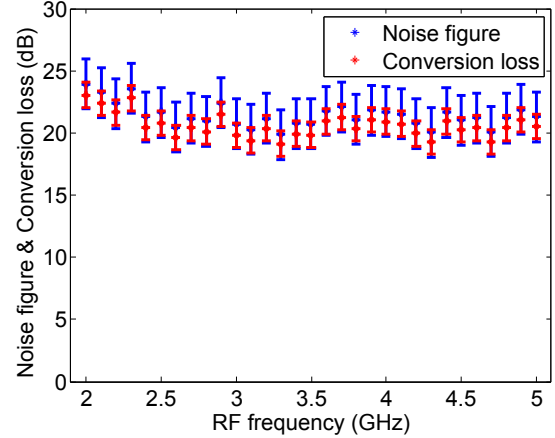

Fig. 5: Conversion loss and SSB noise figure of the device #1 G-FET resistive mixer versus RF frequency. The measurement is performed at room temperature. The error bars correspond to ± 2 dB and ± 1 dB, respectively.

noise figure was analyzed with the attenuator noise model for passive mixers [23]. For a FET resistive mixer, in the absence of gate leakage current, the noise is generally entirely thermal. The model establishes that under these conditions the noise temperature is dependent only upon conversion loss, assumed to be L_{mixer} for both sidebands, and physical temperature, T_p, as

$$T_{mixer,SSB} = T_p \cdot (L_{mixer} - 2). \tag{5}$$

In the ideal case where both RF and image sidebands are down-converted with the same conversion loss, it is valid that $T_{SSB} = 2 \cdot T_{DSB}$. The definition of noise figure for mixers is ambiguous, although the most relevant relation to noise temperature is given by

$$F_{mixer,SSB} = 2 + \frac{T_{mixer,SSB}}{T_0}. \tag{6}$$

The main benefit of (6), where $T_0 = 290$ K, is that it preserves the relation from SSB and DSB noise temperatures, such that $F_{SSB} = 2 \cdot F_{DSB}$, as utilized above to convert the noise figure from DSB to SSB. At room temperature, where $T_p = T_0$, inserting (5) into (6) translates finally into $F_{mixer,SSB} = L_{mixer}$. The result of Fig. 5 is thus a confirmation of the noise to be essentially thermal in a graphene FET resistive mixer, true for e.g. a GaAs fundamental resistive mixer [26] and CMOS subharmonic resistive mixer [27].

Hence, an evident approach to improve the noise figure is to reduce the conversion loss, as for every passive mixer. It should also be possible to cool the mixer to low temperatures, with a greater improvement as compared to e.g. Schottky mixer diodes which are then limited by shot noise [28]. A Y-factor measurement with a combination of high loss and low noise figure would, though, result in an unacceptable uncertainty and was therefore not conducted at this stage.
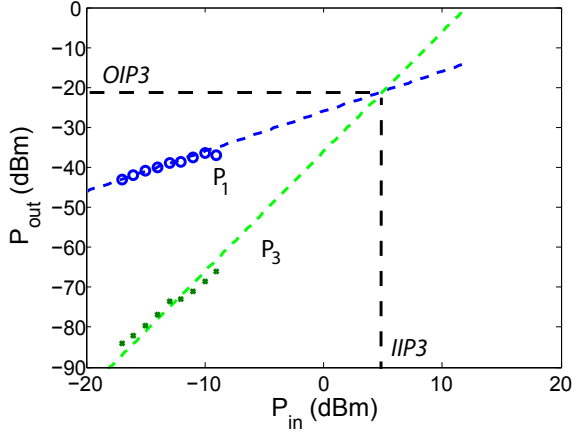
Fig. 6: Linear and third order response for device #2 at 2 GHz, $V_{gs} = V_{dirac}$ and $P_{LO} = 2$ dBm with $IIP3 = 4.9$ dBm.

TABLE II: Measured *IIP3* at $V_{gs} = V_{dirac}$ and $P_{LO} = 0$ dBm

f_{RF}	2 GHz	3 GHz	4 GHz
IIP3	2.9 dBm	3.9 dBm	3.9 dBm

B. Mixer intermodulation

The two-tone measurements for device #2 are summarized in Table II-III versus RF frequency and LO pump power level. Results for device #2 at 2 GHz are presented in Fig. 6, with the linear and third order responses (error ± 0.5 dB for both). To deduce the third order intercept point the regression analysis enforces a slope of one for the linear response and a slope of three for the third order response. The highest measured value for the G-FET subharmonic resistive mixer is *IIP3* = 4.9 dBm at $P_{LO} = 2$ dBm at $f_{RF} = 2$ GHz.

Although it is possible to have single-device, balanced designs [29], the comparison to earlier work considers single-ended *fundamental* resistive FET mixers as presented in Table IV. On one side, for high power handling GaN and SiC FETs [30], [31] *IIP3* values in excess of 30 dBm have been reported. These, however, come at the expense of 23-27 dBm LO power. On the other hand, in CMOS *IIP3* of 16.5 dBm has been achieved with 4 dBm LO power [32]. In between, GaAs single-ended resistive mixers achieve *IIP3* = 28 dBm with $P_{LO} = 10$ dBm [26]. Another way of comparing to reported work in the literature is the use of *IIP3* quality factor, $Q(IIP3) = IIP3/P_{LO}$, also shown in Table IV. For our G-FET mixer, the maximum *Q(IIP3)* = 3.9 dB, from Table II.

Further, the comparison of *IIP3* to *subharmonic* FET resistive mixers (although more seldom reported in the literature) has to consider more complex design architectures, since the single-ended subharmonic mixer is a novel G-FET concept. The IMD is generally worse, with e.g. a single-balanced CMOS mixer reaches *IIP3* = 14 dBm and *Q(IIP3)* = 7 dB at a CL of 12 dB [27].

In order to evaluate the IMD results, two-tone harmonic balance simulations were conducted with the large signal model presented in [21]. The gate bias voltage was varied and the measured and simulated linear and third order responses were compared. The results at $V_{gs} = V_{dirac}$ are compared in

TABLE III: Measured *IIP3* at $V_{gs} = V_{dirac}$ and $f_{RF} = 2$ GHz

P_{LO}	-2 dBm	0 dBm	+2 dBm
IIP3	1.7 dBm	2.9 dBm	4.9 dBm

TABLE IV: Comparison of the G-FET subharmonic mixer with fundamental single-ended resistive mixers

Parameter	[26]	[30]	[31]	[32]	This work
Technology	GaAs	GaN	SiC	CMOS	G-FET
CL (dB)	6.5	6.9	10.2	11.6	20
P_{LO} (dBm)	10	23	27	4	0
f_{RF} (GHz)	10	11	3	60	2-5
IIP3 (dBm)	28	30	35.7	16.5	3.9
Q(IIP3) (dB)	18	7	8.7	12.5	3.9

Fig. 7. This was performed for device #3, which exhibited a symmetric transfer characteristic and therefore only one branch was considered. The measured and simulated results for *IIP3* are given in Table V. A slightly higher value of $P_{LO} = 0.75$ dBm was used for this measurement to provide a comparable R_{on}, despite the lower mobilities (compare Table I). Clearly, at $V_{gs} = V_{dirac}$ the results from the model agree excellently with measurements. On the other hand, away from the Dirac voltage the model tends to overestimate the third order IMD response, leading to a lower *IIP3* point. A complete linear response comparison, showing the rapidly increasing conversion loss with a bias deviating from the Dirac voltage, is presented in Table VI, with good agreement. The discrepancy that exists is partly attributed to an error in the estimated losses in the RF and IF paths of the measurement setup. These results are in line with similar HEMT/MESFET models [33].

To improve the *IIP3* of future G-FET resistive mixers, operation at higher LO power is preferred, as observed in the literature for resistive mixers, the trend in Table III, as well as in Section VI. Also, conventional FET resistive mixers biased at zero drain voltage operate in a linear regime in gate source voltage. The introduction of the resistive mixer was partly motivated by the fact that also a time-varying *linear* element can be used for mixing [26], with improved intermodulation performance. This can be understood by describing the output voltage as a general nonlinear network in terms of a Taylor series in input voltage,

$$v_o = v_o(0) + \frac{v_o'}{1} v_i + \frac{v_o''}{2} v_i^2 + \frac{v_o^{(3)}}{6} v_i^3 + \cdots. \qquad (7)$$

With a two-tune input at frequencies f_1 and f_2 the cubed term of (7) results in the harmful third-order intermodulation products $2f_1 - f_2$ and $2f_2 - f_1$, which are virtually impossible to filter out. By the use of a linear mixing network these frequency products can be suppressed.

The current G-FET resistive mixers, though, have an $R_{ds}(t)$ shape for each branch that is not linear, but instead saturates at higher gate bias as limited by the parasitic resistances. To make the resistance for each branch more linear a decrease of the parasitic resistances is thus an important step. This is further discussed in Section VI.
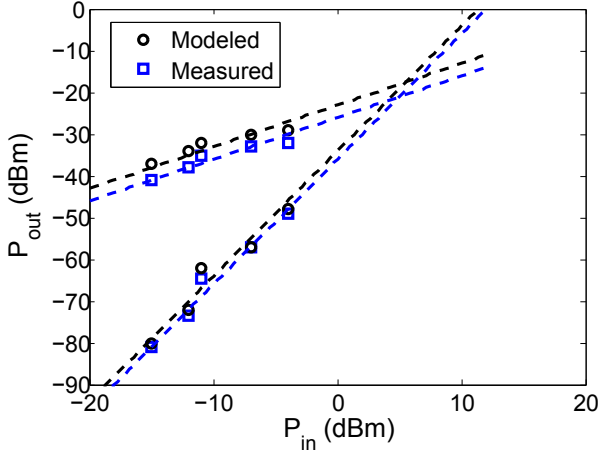
Fig. 7: Measured and modeled linear and third order response for device #3 at 2 GHz, $V_{gs} = V_{dirac}$ and $P_{LO} = 0.75$ dBm.

TABLE V: Comparison between measured and simulated *IIP3* for device #3 at $f_{RF} = 2$ GHz and $P_{LO} = 0.75$ dBm

V_{gs}	V_{dirac}	V_{dirac} - 0.25 V	V_{dirac} - 0.5 V
IIP3 (measured)	4.9 dBm	5.5 dBm	4.6 dBm
IIP3 (simulated)	5.5 dBm	3.3 dBm	1.3 dBm

C. Discussion about mixer conversion loss

The reduction of contact- and access resistances also helps to reduce R_{min}, especially it yields $R_{min} << Z_0$ (typically 50 Ω), to make $\Gamma_{min} \rightarrow -1$. To improve the conversion loss for the resistive mixer application, the introduction of a bandgap in single-layer graphene is not crucial for the purpose of achieving current saturation in the G-FET. Instead, it is important to have $R_{max} >> Z_0$ to make $\Gamma_{max} \rightarrow 1$ and also so that the on and off states can have a more equal duration in time. Together, these steps will make $\Gamma(t)$ resemble a 0.5 duty-cycle square wave and help minimize the conversion loss.

Moreover, lower contact- and access resistances and the introduction of a bandgap would improve the device transconductance. This makes it more suitable for transconductance mixing with the prospect of achieving higher conversion gain in future G-FET mixers. In this context, increased mobility is of course an important step towards improved performance.

VI. FUTURE PERFORMANCE PREDICTION

In order to predict the possible future performance of the G-FET subharmonic mixer, simulations were performed when biased at the Dirac voltage for optimum conversion loss. The model confirms that higher LO power is a general route to improved *IIP3*, as seen from Fig. 8. In order to reduce the demands on LO power, increased mobilities are essential for a steeper transfer characteristic, to change from R_{max} to R_{min} with a smaller voltage swing. Furthermore, concerning a lowered contact resistance, R_c, the results from the simulations partly contradict the claim of Section V-B, which is attributed to a simultaneously improved conversion loss, presented in Fig. 9. This yields higher amplitudes for the down-converted signals at frequencies $f_{IF,1}$ and $f_{IF,2}$ and consequently higher

TABLE VI: Comparison between measured and simulated CL for device #3 at $f_{RF} = 2$ GHz and $P_{LO} = 0.75$ dBm

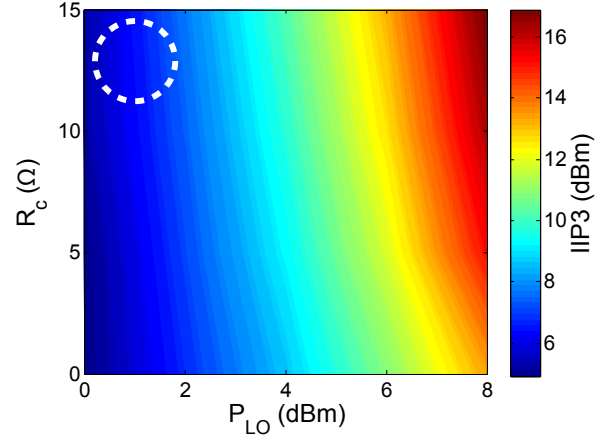| V_{gs}	V_{dirac}	V_{dirac} - 0.25 V	V_{dirac} - 0.5 V
CL (measured)	25 dB	34 dB	38 dB
CL (simulated)	23 dB	36 dB	38 dB

Fig. 8: Modeled *IIP3* versus P_{LO} and R_c at the Dirac voltage $V_{gs} = V_{dirac}$. Measured performance in this work encircled.

power, P_3, for the third order intermodulation products. The results on conversion loss translate also to noise figure, due to the thermal noise with $F_{mixer,SSB} = CL$. Finally, combining the simulated *IIP3* and *CL* data, the mixer spurious free dynamic range (up to the P_{in} where P_3 reaches the noise floor) is calculated [34] according to (8), assuming unity SNR at the mixer output, and presented in Fig. 10. In (8) , N_0 is the output noise power assuming a $BW = 100$ MHz. The performance of the devices presented in this work, with good agreement between experimental and simulated results, is encircled in Fig. 8 through Fig. 10, with a current $DR_f \approx 52$ dB. From Fig. 10, this can be improved significantly at higher LO power. Operation at higher LO power, though, requires an improved gate oxide quality to prevent gate current conduction.

$$DR_f = \frac{2}{3}\left(IIP3 + CL - N_0\right) \qquad (8)$$

VII. CONCLUSION

The first noise figure measurement and IMD analysis of a subharmonic resistive G-FET mixer have been conducted and reported. The devices exhibit state-of-the-art performance for graphene based mixers concerning LO power requirement and conversion loss. The noise was determined to be essentially thermal. Future low temperature experiments will clarify possible departure from thermal noise. Nevertheless, it is important to address the issue of high conversion loss to realize a practical G-FET mixer, e.g. for receiver sensitivity.

Accomplishing a lower conversion loss of the mixer includes an increased on-off ratio, by decreasing parasitic resistances and introducing a bandgap in graphene, as well as devices operating at higher LO power. The latter makes the subharmonic mixer operation more linear to keep the *IIP3* advantage of resistive mixers to active mixers. A bandgap
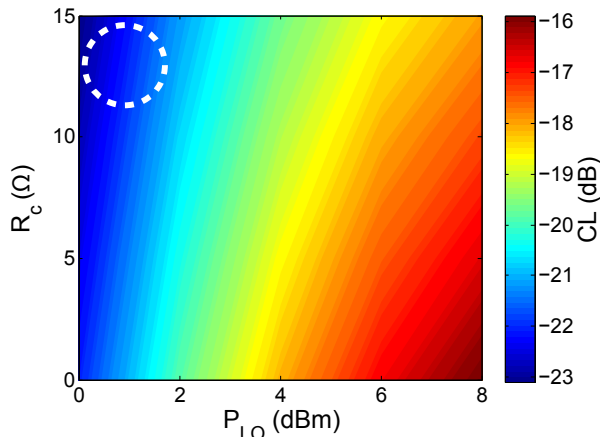
Fig. 9: Modeled CL versus P_{LO} and R_c at the Dirac voltage $V_{gs} = V_{dirac}$. Measured performance in this work encircled.
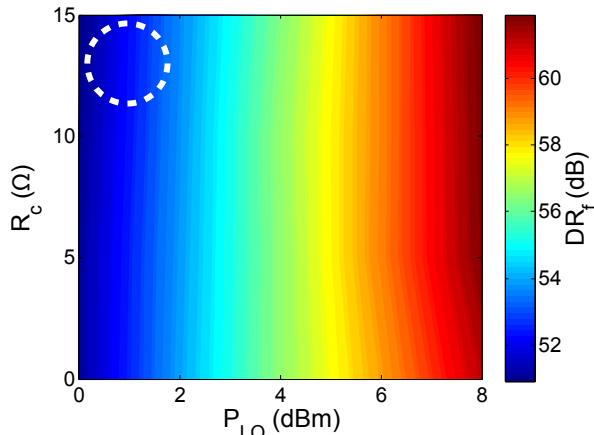

Fig. 10: Modeled DR_f versus P_{LO} and R_c at the Dirac voltage $V_{gs} = V_{dirac}$. Measured performance in this work encircled.

formation helps to have a, for lower conversion loss, beneficial shape of R_{ds}. If these important steps can be achieved, the G-FET resistive subharmonic mixer can be competitive with CMOS counterparts concerning both performance and cost.

ACKNOWLEDGMENT

REFERENCES

[1] S. Cha, J. H. Choi, C. W. Baik, H. B. Sohn, J. Choi, O. Kim, and J. M. Kim, "Perspectives on Nanotechnology for RF and Terahertz Electronics," *IEEE Transactions on Microwave Theory and Techniques*, vol. 59, no. 10, pp. 2709-2718, Oct. 2011.
[2] S. O. Koswatta, A. Valdes-Garcia, M. B. Steiner, Y.-M. Lin, and P. Avouris, "Ultimate RF Performance Potential of Carbon Electronics," *IEEE Transactions on Microwave Theory and Techniques*, vol. 59, no. 10, pp. 2739-2750, Oct. 2011.
[3] K. S. Novoselov, A. K. Geim, S. V. Morozov, D. Jiang, Y. Zhang, S. V. Dubonos, I. V. Grigorieva, and A. A. Firsov, "Electric Field Effect in Atomically Thin Carbon Films," *Science*, vol. 306, no. 5659, pp. 666-669, Oct. 2004.
[4] J.-S. Moon, and D. K. Gaskill "Graphene: Its Fundamentals to Future Applications," *IEEE Transactions on Microwave Theory and Techniques*, vol. 59, no. 10, pp. 2702-2708, Oct. 2011.
[5] F. Bonaccorso, Z. Sun, T. Hasan, and A. C. Ferrari, "Graphene photonics and optoelectronics," *Nature Photonics*, vol. 4, pp. 611-612, Aug. 2010.
[6] F. Schedin, A. K. Geim, S. V. Morozov, E. W. Hill, P. Blake, M. I. Katsnelson, and K. S. Novoselov, "Detection of individual gas molecules adsorbed on graphene," *Nature Materials*, vol. 6, pp. 652-655, Jul. 2007.
[7] M. C. Lemme, T. J. Echtermeyer, M. Baus, and H. Kurz, "A Graphene Field-Effect Device," *IEEE Electron Device Letters*, vol. 28, no. 4, pp. 282-284, Apr. 2007.
[8] Y. Q. Wu, D. B. Farmer, A. Valdes-Garcia, W. J. Zhu, K. A. Jenkins, C. Dimitrakopoulos, P. Avouris, and Y.-M. Lin, "Record high RF performance for epitaxial graphene transistor," in *IEEE International Devices Meeting*, pp. 23.8.1-23.8.3, Dec. 2011.
[9] H. Wang, A. Hsu, J. Wu, J. Kong, and T. Palacios, "Graphene Frequency Multipliers," *IEEE Electron Device Letters*, vol. 30, no. 5, pp. 547-549, 2009.
[10] H. Wang, A. Hsu, J. Wu, J. Kong, and T. Palacios, "Graphene-Based Ambipolar RF Mixers," *IEEE Electron Device Letters*, vol. 31, no. 9, pp. 906-908, 2010.
[11] Y.-M. Lin, A. Valdes-Garcia, S. Han, D. B. Farmer, I. Meric, Y. Sun, Y. Wu, C. Dimitrakopoulos, A. Grill, P. Avouris, and K. A. Jenkins, "Wafer-Scale Graphene Integrated Circuit," *Science*, vol. 332, no. 6035, pp. 1294-1297, Jun. 2011.
[12] O. Habibpour, S. Cherednichenko, J. Vukusic, K. Yhland, and J. Stake, "A Subharmonic Graphene FET Mixer," *IEEE Electron Device Letters*, vol. 33, no. 1, pp. 71-73, Jan. 2012.
[13] M. A. Andersson, O. Habibpour, J. Vukusic, and J. Stake, "A 10-dB Small-Signal Graphene FET Amplifier," *Electron. Lett.*, vol. 48, no. 14, pp. 861-863, Jul. 2012.
[14] G. Deligiorgis, F. Coccetti, G. Konstantinidis, and R. Plana, "Radio frequency signal detection by ballistic transport in Y-shaped graphene nanoribbons," *Applied Physics Letters*, vol. 101, 013502, 2012.
[15] S. A. Maas, *Nonlinear Microwave and RF Circuits*, Artech House, 2005.
[16] K. Yhland, "Simplified Analysis of Resistive Mixers," *IEEE Microwave and Wireless Component Letters*, vol. 17, no. 8, pp. 604-606, Aug. 2007.
[17] A. J. Kelly, "Fundamental Limits on Conversion Loss of Double Sideband Resistive Mixers" *IEEE Transactions on Microwave Theory and Techniques*, vol. 25, no. 11, pp. 867-869, Nov. 1977.
[18] H. Zirath, "Subharmonically Pumped Resistive Dual-HEMT-Mixer," in *IEEE MTT-S Int. Microw. Symp. Dig.* Jul. 1991, pp. 875-878.
[19] M. Andersson, O. Habibpour, J. Vukusic, and J. Stake, "Noise Figure Characterization of a Subharmonic Graphene FET Mixer," in *IEEE MTT-S Int. Microw. Symp. Dig.*, Montreal, Jun. 2012, pp. 1-3.
[20] J. S. Moon, D. Curtis, D. Zehnder, S. Kim, D. K. Gaskill, G. G. Jernigan, R. L. Myers-Ward, C. R. Eddy, P. M. Campbell, K.-M. Lee, and P. Asbeck, "Low-Phase-Noise Graphene FETs in Ambipolar RF Applications," *IEEE Electron Device Letters*, vol. 32, no. 3, pp. 270-272, March 2011.
[21] O. Habibpour, J. Vukusic, and J. Stake, "A Large Signal Graphene FET Model," *IEEE Transactions on Electron Devices*, vol. 59, no. 4, pp. 968-975, Apr. 2012.
[22] R. A. Pucel, D. Masse, and R. Bera, "Performance of GaAs MESFET Mixers at X Band," *IEEE Transactions on Microwave Theory and Techniques*, vol. 24, no. 6, pp. 351-360, Jun. 1976.
[23] S. A. Maas, *Noise in Linear and Nonlinear Circuits*, Artech House, 2005.
[24] L. Liao, J. Bai, R. Cheng, H. Zhou, L. Liu, Y. Liu, Y. Huang, and X. Duan, "Scalable fabrication of self-aligned graphene transistors and circuits on glass," *Nano Letters*, vol. 12, no. 6, pp. 2653-2657, Jun. 2011.
[25] "Noise Figure Measurement Accuracy - The Y-Factor Method," *Agilent Application Note*, 2010, 57-2.
[26] S. A. Maas, "A GaAs MESFET Mixer with Very Low Intermodulation," *IEEE Transactions on Microwave Theory and Techniques*, vol. 35, no. 4, pp. 425-429, Apr. 1987.
[27] H.-J. Wei, C. Meng, P.-Y. Wul, and K.-C. Tsung, "K-Band CMOS Sub-Harmonic Resistive Mixer With a Miniature Marchand Balun on Lossy Silicon Substrate', *IEEE Microwave and Wireless Components Letters*, vol. 18, no. 1, pp. 40-42, Jan. 2008.
[28] A. van der Ziel, "Theory of Shot Noise in Junction Diodes and Junction Transistors," *Proceedings of the IRE*, vol. 43, no. 11, pp. 1639-1646, Nov. 1955.

[29] K. Yhland, N. Rorsman, and H. Zirath, "Novel Single Device Balanced Resistive HEMT Mixers," *IEEE Transactions on Microwave Theory and Techniques*, vol. 43, no. 12, pp. 2863-2867, Dec. 1995.

[30] M. Sudow, K. Andersson, M. Fagerlind, M. Thorsell, P.-A Nilsson, and N. Rorsman, "A Single-Ended Resistive X-Band AlGaN/GaN HEMT MMIC Mixer," *IEEE Transactions on Microwave Theory and Techniques*, vol. 56, no. 10, pp. 2201-2206, Oct. 2008.

[31] K. Andersson, J. Eriksson, N. Rorsman, and H. Zirath, "Resistive SiC-MESFET Mixer," *IEEE Microwave and Wireless Component Letters*, vol. 12, no. 4, pp. 119-121, Apr. 2002.

[32] B. M. Motlagh, S. E. Gunnarsson, M. Ferndahl, and H. Zirath, "Fully integrated 60-GHz single-ended resistive mixer in 90-nm CMOS technology', *IEEE Microwave and Wireless Components Letters*, vol. 16, no. 1, pp. 25-27, Jan. 2006.

[33] K. Yhland, N. Rorsman, M. Garcia, and H. F. Merkel, "A Symmetrical Nonlinear HFET/MESFET Model Suitable for Intermodulation Analysis of Amplifiers and Resistive Mixers', *IEEE Transactions on Microwave Theory and Techniques*, vol. 48, no. 1, pp. 15-22, Jan. 2000.

[34] D. M. Pozar, *Microwave and RF Design of Wireless Systems*, Wiley, 2001.

Michael Andersson (S'12) was born in Varberg, Sweden 1988. He received the B.S. and M.Sc. degrees in electrical engineering from Chalmers University of Technology, Göteborg, Sweden in 2010 and 2012, respectively. He is currently with the Terahertz and Millimetre Wave Laboratory, Department of Microtechnology and Nanoscience (MC2), Chalmers University of Technology, Göteborg, Sweden, where he is working towards a Ph.D. degree in graphene electronics for high-frequency applications.

Omid Habibpour (S'08) received the B.S. degree in electrical engineering from Sharif University of Technology, Tehran, Iran, in 2002 and the M.S. degree in electrical engineering from Amirkabir University of technology, Tehran, Iran, in 2004. He is currently working towards the Ph.D. degree in graphene electronics with the Terahertz and Millimetre Wave Laboratory, Department of Microtechnology and Nanoscience, Chalmers University of Technology, Göteborg, Sweden.

Josip Vukusic (M'11) received the diploma and Ph.D. degree in photonics from Chalmers University of Technology, Göteborg, Sweden, in 1997 and 2003, respectively. Since 2004, he has been with the Terahertz and Millimetre Wave Laboratory, Department of Microtechnology and Nanoscience, Chalmers University of Technology, working on terahertz (THz) technology. He is currently involved in modeling, fabrication, and characterization of frequency multipliers for THz generation.

Jan Stake (S'95-M'00-SM'06) was born in Uddevalla, Sweden in 1971. He received the degrees of M.Sc. in electrical engineering and Ph.D. in microwave electronics from Chalmers University of Technology, Göteborg, Sweden in 1994 and 1999, respectively.

In 1997 he was a Research Assistant at the University of Virginia, Charlottesville, USA. From 1999 to 2001, he was a Research Fellow in the millimetre wave group at the Rutherford Appleton Laboratory, UK. He then joined Saab Combitech Systems AB as a Senior RF/microwave Engineer until 2003. From 2000 to 2006, he held different academic positions at Chalmers and was also Head of the Nanofabrication Laboratory at MC2 between 2003 and 2006. During the summer 2007, he was a Visiting Professor in the Submillimeter Wave Advanced Technology (SWAT) group at Caltech/JPL, Pasadena, USA. He is currently Professor and Head of the Terahertz and Millimetre Wave Laboratory at the Department of Microtechnology and Nanoscience (MC2), Chalmers, Göteborg, Sweden. His research involves sources and detectors for terahertz frequencies, high frequency semiconductor devices, graphene electronics, terahertz measurement techniques and applications. He is also co-founder of Wasa Millimeter Wave AB, Göteborg, Sweden.

Prof. Stake serves as Topical Editor for the IEEE Transactions on Terahertz Science and Technology.